iScience

CellPress
OPEN ACCESS

Article

Endocrine disrupting chemicals differentially alter intranuclear dynamics and transcriptional activation of estrogen receptor-α

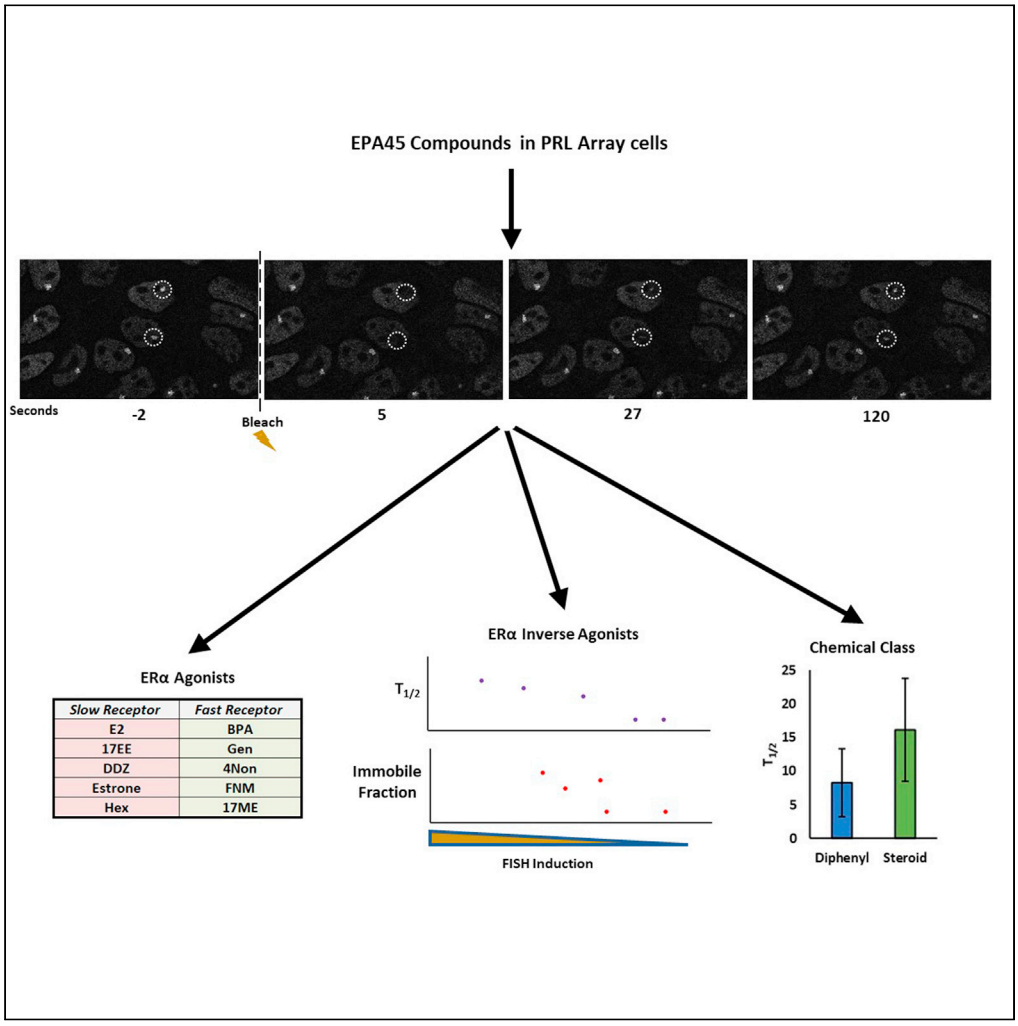

Michael J. Bolt, Pankaj Singh, Caroline E. Obkirchner, ..., Adam T. Szafran, Fabio Stossi, Michael A. Mancini

mancini@bcm.edu

Highlights

Development of a new algorithm for multi-foci FRAP analysis

ERα agonists can be segregated into fast-moving and slow-moving receptor groups

ERα inverse agonists receptor mobility inversely correlates with transcription

Steroidal compounds result in a slower moving receptor than other classes

Bolt et al., iScience *24*, 103227
November 19, 2021
https://doi.org/10.1016/j.isci.2021.103227

iScience

CellPress
OPEN ACCESS

Article

Endocrine disrupting chemicals differentially alter intranuclear dynamics and transcriptional activation of estrogen receptor-α

Michael J. Bolt,[3,4] Pankaj Singh,[3,4] Caroline E. Obkirchner,[3,4] Reid T. Powell,[4] Maureen G. Mancini,[1] Adam T. Szafran,[1] Fabio Stossi,[1,3] and Michael A. Mancini[1,2,3,4,5,*]

SUMMARY

Transcription is a highly regulated sequence of stochastic processes utilizing many regulators, including nuclear receptors (NR) that respond to stimuli. Endocrine disrupting chemicals (EDCs) in the environment can compete with natural ligands for nuclear receptors to alter transcription. As nuclear dynamics can be tightly linked to transcription, it is important to determine how EDCs affect NR mobility. We use an EPA-assembled set of 45 estrogen receptor-α (ERα) ligands and EDCs in our engineered PRL-Array model to characterize their effect upon transcription using fluorescence *in situ* hybridization and fluorescence recovery after photobleaching (FRAP). We identified 36 compounds that target ERα-GFP to a transcriptionally active, visible locus. Using a novel method for multi-region FRAP analysis we find a strong negative correlation between ERα mobility and inverse agonists. Our findings indicate that ERα mobility is not solely tied to transcription but affected highly by the chemical class binding the receptor.

INTRODUCTION

Estrogen receptor-α (ERα) is a prototypical steroid receptor and member of the nuclear receptor (NR) superfamily that can act as a transcription factor regulating gene transcription in response to hormones produced by the endocrine system. ERα is a central transcriptional modulator that plays important pathophysiological roles in multiple tissues, including mammary gland (Vasquez, 2018), uterus (Horner-Glister et al., 2005), and bone (Rudnik et al., 2008). The endogenous ligand for ERα is 17β-estradiol (E2), a steroid synthesized from androgen precursors through the enzyme aromatase (Simpson et al., 1994). Targeted therapeutics, including 4-hydroxytamoxifen (4HT) and other selective estrogen receptor modulators (SERMs) and degraders (SERDs), have been used to compete with E2 and turn off activity, or degrade the receptor, blocking its pro-proliferative program (Powles, 2006). Since the industrial age began, runoff from commercial processes has introduced numerous chemicals (such as bisphenol A, BPA) into the environment that can activate or inactivate ERα; unfortunately, most of these chemicals have not been fully tested.

Endocrine disrupting chemicals (EDCs) are compounds that can alter hormone-responsive cells and tissues by frequently binding nuclear receptors (Zoeller et al., 2012). EDCs have been associated in epidemiological studies with a wide variety of pathological conditions including cancer, metabolic and developmental defects (De Coster and van Larebeke, 2012; Rochester, 2013). These compounds are diverse in chemical structure, produced either naturally through metabolism of exogenous chemicals or through industrial sources. Such compounds have been tested primarily in biochemical assays to determine which nuclear receptors or pathways are involved, indicating that estrogen, androgen, and thyroid receptors are the primary, but not the only target of EDCs. Although high throughput/high content assays have been utilized in the past to define mechanistic characteristics of EDCs (Stossi et al., 2014; Kornhuber et al., 2021; Stavreva et al., 2016), their influence on receptor structure and function have not been fully assessed. In response, the Environmental Protection Agency (EPA) identified a set of 45 ERα positive (agonists and antagonists) and negative reference (Judson et al., 2015) compounds (EPA45) to facilitate and expand research in this area. The EPA45 includes well known natural ligands of ERα, and common EDCs such as BPA. The use of these chemicals in a suite of estrogen response assays provides an excellent starting point for

[1]Department of Molecular and Cellular Biology, Baylor College of Medicine, Houston, TX 77030, USA

[2]Department of Pharmacology and Chemical Biology, Baylor College of Medicine, Houston, TX 77030, USA

[3]Center for Advanced Microscopy and Image Informatics, Institute of Biosciences & Technology, Texas A&M University, Houston, TX 77030, USA

[4]Center for Translational Cancer Research, Institute of Biosciences & Technology, Texas A&M University, Houston, TX 77030, USA

[5]Lead contact

*Correspondence: mancini@bcm.edu

https://doi.org/10.1016/j.isci.2021.103227

many lines of mechanistic EDC research. One aspect missed by all current ToxCast assays is the effect of a chemical on ERα mobility within nuclei, even though this has been shown to directly affect downstream mechanistic steps including DNA binding residency time and gene transcription (Stenoien et al., 2001a).

Fluorescence recovery after photo bleaching (FRAP) utilizes time-lapse imaging and a fluorescently tagged molecule to determine mobility of proteins within a given system. This approach has been widely used to study protein dynamics in the context of living cells (van Royen et al., 2009) as multiple studies have found a strong link between transcription factor mobility and transcription factor function (Govindaraj et al., 2019; Stenoien et al., 2001a). Previous FRAP on ERα (Amita et al., 2010; Damdimopoulos et al., 2008) demonstrated a rapidly moving receptor within the nucleus under control conditions (no ligand added) and decreased mobility upon E2 or 4HT treatment, owing, in part, to the receptor binding to DNA, protein-protein interactions, and ill-defined nuclear structures (i.e., nucleoskeleton/nuclear matrix). Interestingly, the selective estrogen receptor degrader, ICI182,780 (ICI, also known clinically as Fulvestrant), caused marked immobilization of ERα, perhaps linked to ubiquitinylation and proteasome degradation (Stenoien et al., 2001a). Recently, a second structurally similar ligand (GDC-0927) was found to immobilize and degrade ERα in a similar fashion to ICI (Guan et al., 2019). Despite the utilization of FRAP to study GFP-ERα during the last two decades, only a handful of compounds have ever been tested, and generally with only a minimal number of replicates and cells/treatment. Here, we define the range and scale of altered nuclear mobility changes possible for ERα-GFP when exposed to the EPA45 chemical library. In addition, we sought to determine whether specific classes of compounds are linked to the results of other mechanistic steps, including chromatin remodeling and gene transcription.

In previous studies, we have utilized an engineered ERα model that is amenable to high throughput, high content analysis due to a multicopy integration of an ERE-rich modified prolactin (PRL) reporter gene that forms a ligand-dependent, visible nuclear spot that is easily detectable (~1 micron in size) by fluorescent microscopy, here called "arrays" (Bolt et al., 2013, 2015; Sharp et al., 2006). Owing to the multiple mechanistic endpoints that are available from fixed or live PRL-HeLa experiments, we chose to perform FRAP experiments with the EPA45 compound set and a recently modified PRL-array cell line that is now doxycycline-regulated, ERα-GFP:PRL-HeLa (PRL-Array), and analyzed with a new Python-based method to decrease the time for multiple ROI measurements. We combined these findings with the more classical metrics of the standard PRL-Array assay, including transcriptional output by mRNA fluorescence *in situ* hybridization (FISH) and chromatin remodeling ("array size"). Here, our efforts confirm the high mobility of nuclear ERα-GFP under untreated conditions, slowed ERα dynamics by E2 treatment, and its immobilization by ICI. We also show that across a group of inverse agonist compounds, slower mobility of the receptor correlates with a marked reduction of transcription output. Finally, we observe differences in ERα mobility between compounds that are classified by chemical structure. Taken together, we find that ERα mobility is not solely tied to transcription but affected highly by the chemical class that binds the receptor.

RESULTS

Profiling the EPA45 compounds in a new dox-inducible PRL-array cell line

We utilized a modified version of our previously published GFP-ERα:PRL-HeLa (iERα-GFP or PRL-array) cell line to measure the effects of a set of estrogenic compounds assembled by the EPA. As with the previously used PRL-HeLa cells (GFP-ERα), the parental HeLa cell line contains ~100 copies of a modified prolactin reporter gene that includes a 'synergy element' in the distal enhancer containing a full and half estrogen response element that was reiterated 52x to create a super enhancer driving expression of dsRed2 (ref). Unlike the original double-stable GFP-ERα:PRL-HeLa line (Sharp et al., 2006), we used a dox-inducible, C-terminal fusion of ERα (ERα-GFP) that behaves similarly following hormone stimulation, causing a visible nuclear spot to appear as ERα-GFP specifically targets the EREs in the multicopy reporter gene locus. We utilize this new cell line for multiple reasons. The original cell line (GFP-ERα:PRL-HeLa)_was CMV promoter-regulated, expressing GFP-ERα at levels several-fold higher than MCF-7 cells whereas the new array line (iERα-GFP:PRL-HeLa) can be tuned to express lower ERα-GFP expression (~50% less expression, Figure S1A). Also, the original GFP-ERα:PRL-HeLa cells also had to be treated in tamoxifen to avoid reduced growth while expanding cultures as GFP-ERα expression would cause the cells to stop replicating, even without E2. The iERα-GFP:PRL-HeLa cells have no such restriction as treatment with doxycycline can bring the expression to usable levels in just 24 h. This also makes the cell line more sensitive to hormone levels, as iERα-GFP:PRL-HeLa cells cause array formation with less E2 than GFP-ERα:PRL-HeLa (Figure S1B). Finally, we see higher levels of reporter gene (dsRed2) mRNA production following hormone induction, in the

Table 1. The compounds in the EPA45 compound set

Compound	Abbreviation	Class	Conc. (uM)
17alpha-estradiol	17a	Steroid	0.01
17alpha-ethinylestradiol	17EE	Steroid	0.01
17beta-estradiol	E2	Steroid	0.01
4-Hydroxytamoxifen	4HT	Oxifen	0.01
Diethylstilbestrol	DES	Stilbestrol	0.01
Estrone	Est	Steroid	0.01
Genistein	Gen	Isoflavone	0.01
meso-Hexestrol	Hex	Stilbestrol	0.01
Raloxifene hydrochloride	Ral	Oxifen	0.01
Tamoxifen	Tam	Oxifen	0.01
Tamoxifen citrate	TamC	Oxifen	0.01
4-(1,1,3,3-tetramethylbutyl) phenol	413P	Phenol	0.1
4-Cumylphenol	4Cum	Diphenyl	0.1
Bisphenol A	BPA	Diphenyl	0.1
Bisphenol B	BPB	Diphenyl	0.1
Fenarimol	FNM	Diphenyl	0.1
Kaempferol	KMF	Isoflavone	0.1
Phenobarbitol sodium	PHB	Barbiturate	0.1
17-Methyltestosterone	17ME	Steroid	1
5alpha-dihydroxytestosterone	DHT	Steroid	1
Benzylbutyl phthalate	BBP	Phthalate	1
Daidzein	DDZ	Isoflavone	1
Kepone	KP	Organochlorine	1
Methoxychlor	MOC	Diphenyl	1
o'p'-DDT	DDT	Diphenyl	1
4-Nonylphenol	4Non	Phenol	10
Apigenin	APE	Isoflavone	10
Corticosterone	Cort	Steroid	10
Dibutyl Phthalate	DBP	Phthalate	10
Dicofol	Dic	Diphenyl	10
Ethylparaben	EPB	Phenol	10
Hydroxyflutamide	HF	Phenylamine	10
Linuron	Lin	Phenylamine	10
p'p'-DDE	DDE	Diphenyl	10
Progesterone	P4	Steroid	10
Spironolactone	Spiro	Steroid	10
Atrazine	Atz	Triazine	NA
Chrysin	Chr	Isoflavone	NA
Cyclohexamide	CHX	Imide	NA
Di(2-ethylhexyl) Phthalate	DEHP	Phthalate	NA
Flutamide	Flut	Phenylamine	NA
Haloperidol	Hel	Phenylacetone	NA
Ketoconazole	Keto	Azole	NA

(*Continued on next page*)

Table 1. *Continued*

Compound	Abbreviation	Class	Conc. (uM)
Procymidone	Pry	Chlorobenzene	NA
Reserpine	RSP	Steroid	NA

The compounds include the abbreviations, the compound class used for this manuscript, and the lowest dose that could induce maximal array formation in the PRL-Array cell line. This dose was used for all experiments. Compounds with N/A were unable to induce array formation at any concentration tested.

iERα-GFP array line using RNA FISH (Figure S1C). The more physiological level of ERα-GFP, the increased sensitivity and more abundant dsRed2 mRNA make iERα-GFP:PRL-HeLa (from here on called PRL-Array) a better choice for drug screening applications.

Our test bed of analytes was a reference set of known estrogenic and non-estrogenic compounds from the EPA (EPA45 (Judson et al., 2015), Table 1, (compound structures for array-inducing compounds are shown in Figure S2). The EPA45 compounds were initially tested in our PRL-Array cell model to determine their ability to induce array formation. All EPA45 compounds were tested using a four-point dose response (0.01 μM, 0.1 μM, 1 μM, and 10 μM) for 30 min, and we measured the fraction of cells forming a visible nuclear array (Figure 1A, % arrays), chromatin decondensation/condensation (Figure 1B, array area), and transcription induction (Figure 1C, dsRed2 FISH Intensity). Nine of the 45 compounds did not induce array formation above background, at any dose, in agreement with previously published results looking into the estrogenicity of these compounds (Judson et al., 2015). These compounds were considered inactive in this assay at these doses and left out of further analysis.

Similar to our previous studies with the original PRL-Array model, 17β-estradiol (E2) was able to induce large, decondensed arrays at all concentrations tested, and robust mRNA reporter gene (dsRed2) activity. 4-hydroxytamoxifen (4HT) was similar in dose-response, but the arrays were smaller/condensed, and induction of reporter gene mRNA was suppressed, suggesting a classic ERα inverse agonist class of compounds (representative images in Figure S3). Interestingly, we observed array formation by Phenobarbital Sodium (PHB) treatment as low as 0.1μM concentration, which has not been reported in the original ToxCast dataset (Judson et al., 2015). However, we did measure an effect of PHB on endogenous ERα levels in an orthogonal MCF-7 assay, and a recent study showed PHB transcriptional activation in an ERE luciferase assay (Xu et al., 2019). The lowest dose for each compound that induced array formation is listed in Table 1. These data indicate that our ERα assay is capable of recapitulating known ligand effects, and as a discovery tool to identify possible novel ligands. One aspect of ERα activity that many studies fail to address is its intranuclear mobility, which is assessed by fluorescence recovery after photobleaching (FRAP).

Quantitation of multiple FRAP ROIs with FRAPnalysis workflow

To query the effects of the EPA45 compounds on ERα intranuclear mobility, we used FRAP. To improve the efficiency of the analyses, we first developed and validated a Python-based method for FRAP analysis. This approach was used to rapidly identify multiple ROIs and normalize for photobleaching during image acquisition at each ROI, a process we termed FRAPnalysis. After collecting a FRAP image series with bleached ROIs centered on the formed arrays within the PRL-Array cells (Figure 2A, with bleached areas shown by orange arrows), we utilized image math to subtract the last pre-bleach image from the first post-bleach image (Figure 2B). The resulting image is then threshold to determine the FRAP ROI. Nuclei are then segmented based on the GFP signal and a random number of regions are chosen in cells that do not contain a FRAP ROI (Figures S4A and S4B). The random regions are utilized to determine the amount of photobleaching across the FRAP series. The photobleaching measurements are averaged and the correction is applied to the FRAP ROIs and plotted (Figure S4C). The pipeline automatically fits the data to a negative exponential function producing curves for both non-corrected (Figure S4D) and photobleaching corrected data (Figure S4E). We utilized these measurements to determine FRAP curves with 95% confidence intervals for two well-known ERα ligands with opposite effect on mobility, 17β-estradiol (E2, Figure 2C) and ICI-182,780 (ICI, Figure 2D). E2 is the endogenous and most-studied ligand for ERα, and ICI is an ERα degrading ligand known for immobilizing the receptor (Stenoien et al., 2001a, 2001b). Here, we could easily and quickly perform FRAP experiments and analysis on a larger number of cells as compared to most published studies, including several biological replicates indicating good

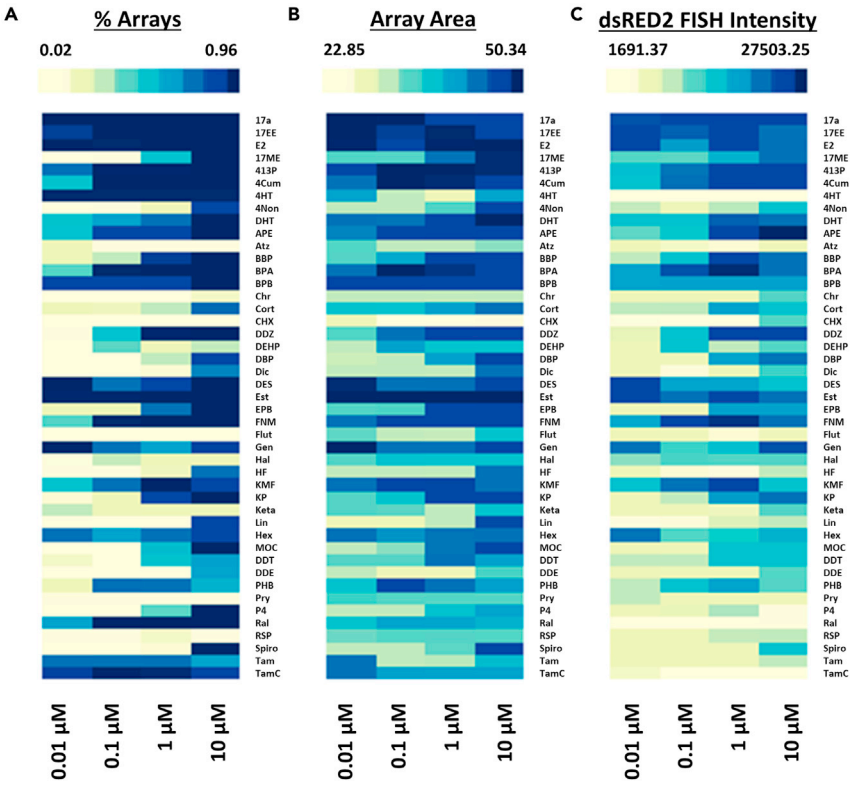

Figure 1. Activity of the EPA45 compounds in the PRL-Array cell line

(A–C) Heat maps for the EPA45 compound dose responses in the PRL-Array cells relating to (A) % of cells with a visible array, (B) array area in pixels, or (C) dsRed2 FISH integrated intensity at the array.

reproducibility of our method. Ultimately, this data indicates how our workflow allows for a higher throughput pipeline to produce FRAP metrics with larger numbers of replicates.

FRAP experiments yield two quantitative metrics: $T_{1/2}$, which measures the speed of half recovery, and immobile fraction, which measures the scale of recovery. These two measurements allow determination of the speed at which the ERα-GFP molecules move and how tightly they are bound to DNA, protein complexes, and/or the nuclear matrix. We next sought to determine whether our pipeline could be used to measure antagonism in a dose dependent manner using the FRAP curves and metrics. To this end, we treated ERα-GFP:PRL-Array cells with a range of ICI182,780 concentrations (100pM–100nM) while maintaining 1nM E2 treatment constant. E2 treatment leads to more cells with a visible array, a larger array area, and more dsRed2 FISH signal than ICI (Figures S5A–S5C, respectively) and previous research has shown that ICI immobilizes ERα (Stenoien et al., 2001b). We observed a successful dose response in the FRAP curves (Figure S5D), immobile fraction (Figure S5E), and $T_{1/2}$ (Figure S5F). Interestingly, we see an intermediate immobile fraction response when treated with 1nM ICI and 1nM of E2, with a shift in the $T_{1/2}$ occurring at 10nM ICI. The shifting of the E2 curve in response to ICI indicates that our assay is capable of identified dose-dependent effects on ERα-GFP.

Comparison of $T_{1/2}$ and immobile fraction using EPA45 compounds

We used the above method to perform a FRAP series using all EPA45 compounds that induced array formation (36 compounds) within the PRL-Array cell model. For each compound we used the lowest dose that induced significant array induction compared to DMSO (see Table 1, concentration used column). Figure 3A is a waterfall plot representing the $T_{1/2}$ for each compound while Figure 3B shows the immobile fraction for each compound. We observed a range of $T_{1/2}$ from rapid recovery of ERα-GFP (min $T_{1/2}$: 2.2s for methoxychlor (MOC)) to very slow moving ERα-GFP (max $T_{1/2}$: 26.41s for E2). The immobile fractions (max: raloxifene hydrochloride (Ral), min: kaempferol (KMF)) showed less variation with most values within

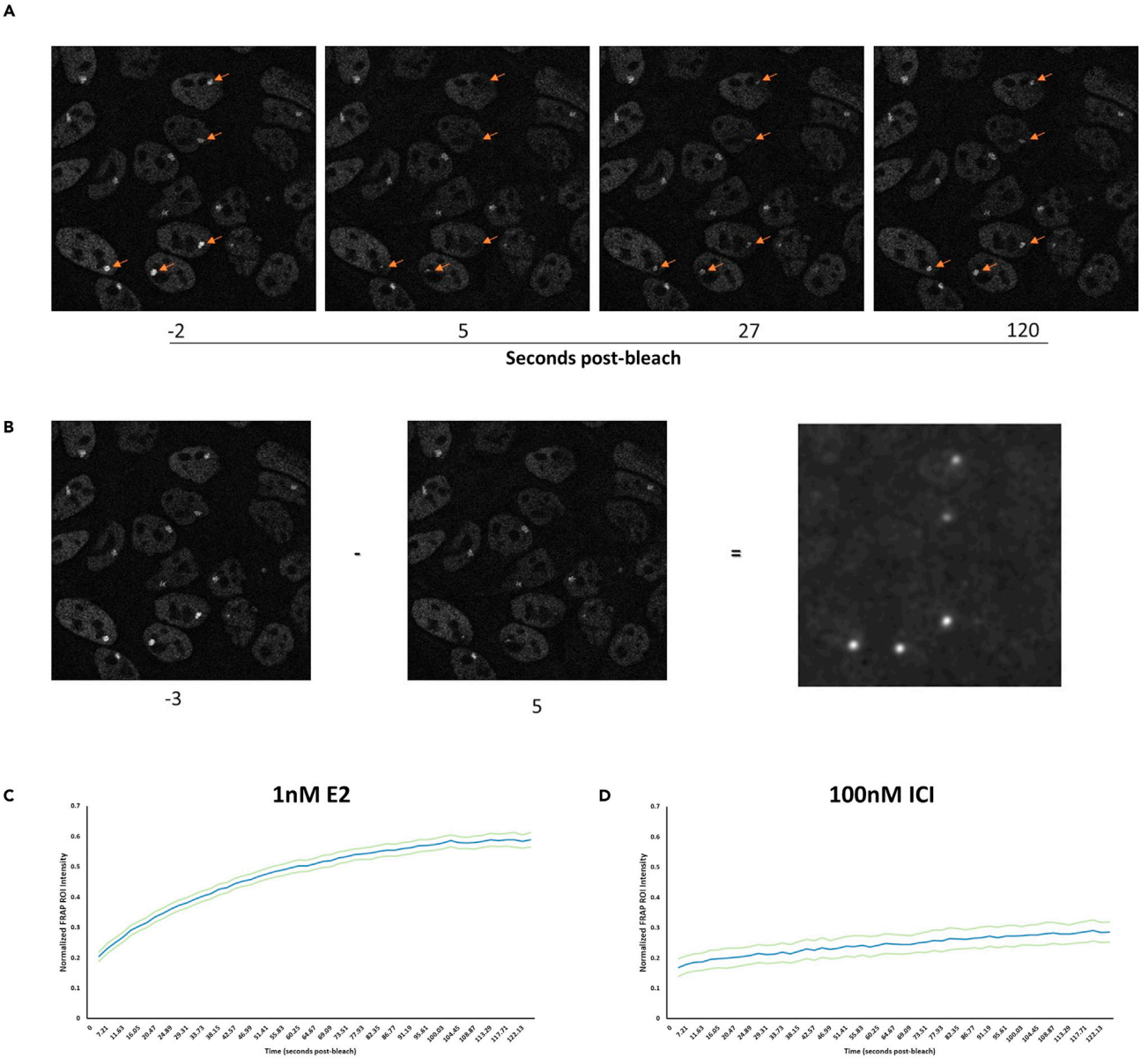

Figure 2. FRAPnalysis workflow

(A) Representative images from distinct time points along the FRAP imaging experimental axis in the PRL-Array cell line. The Array in each nucleus was the chosen region for photobleaching (orange arrows).

(B) Image subtraction of the last pre-bleach image and the first post-bleach image allows for quick discovery of FRAP ROIs. (C-D) Recovery curves with a 95% confidence interval for 17β-estradiol (1nM, n = 46 cells, in 5 biological replicates) and ICI182,780 (n = 25 cells, 3 biological replicates).

one standard deviation of E2. The $T_{1/2}$ of the EPA45 compounds was compared to the immobile fraction (Figure 3D) and a Pearson's correlation of 0.589 was observed. To determine which EPA45 compounds were considered outliers, we utilized an isolation forest model (see STAR Methods). Figure 3C shows the FRAP curves for an average ERα-GFP ligand, which was created in silico by averaging the 30 compounds that the analysis determined not to be outliers) and six outlier chemicals (E2, 17EE, Ral, MOC, KMF, and 17ME; all FRAP curves can be viewed in Figures S6A–S6D grouped by chemical class).

We further wanted to determine whether different classes of compounds, based on chemical structure, exhibited altered the mobility of ERα-GFP. The compounds that caused array formation were grouped by

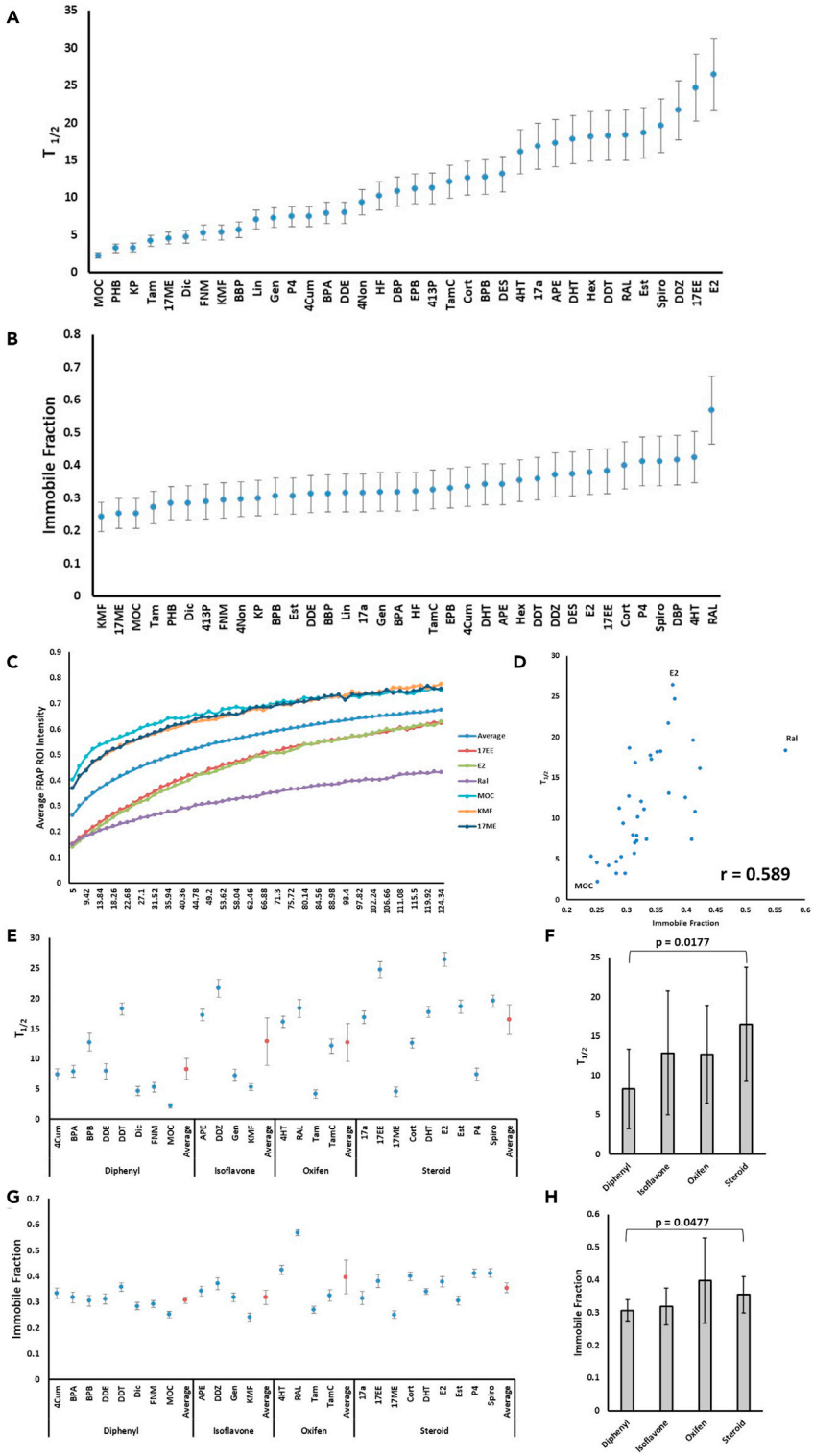

Figure 3. FRAP metrics of the EPA45 compounds that cause formation of a visible nuclear spot

(A) Waterfall plot of EPA45 compounds showing $T_{1/2}$.

(B) Waterfall plot of EPA45 compounds showing immobile fraction.

Figure 3. *Continued*

(C) Average FRAP runs for outlier EPA45 compounds (17-Ethinyestradiol, 17β-Estradiol, Raloxifene Hydrochloride, Methoxychlor, Kaempferol, 17-Methylestosterone) versus the average of non-outlier compounds. Outliers were determined using isolation forest analysis.

(D) Correlation plot of $T_{1/2}$ versus Immobile Fraction.

(E and F) $T_{1/2}$ of four classes of compounds within the EPA45 and their class average.

(G and H) Immobile fraction of four classes of compounds within the EPA45 and their class average. Data are represented as mean ± SD.

common structure and Tanimoto index, which is based on SMILES compound similarity (Ozturk et al., 2016; Bajusz et al., 2015). In the EPA45 list there are 4 classes of compounds with at least four compounds each (diphenyls (8), oxifens (4), isoflavones (4), and steroids (9)). We compared the $T_{1/2}$ (Figures 3E and 3F) and immobile fraction (Figures 3G and 3H) of the individuals of these groups, and the average across the group. We find that the diphenyl compounds (BPA, DDT) on average have a significantly lower $T_{1/2}$ and immobile fraction than the steroidal compounds (E2, DHT). These data suggest a range of mobility and DNA binding effects of the EPA45 compounds on ERα with certain compound classes having greater effect.

$T_{1/2}$ and immobile fraction negatively correlate with efficacy of inverse agonists

We then explored whether the $T_{1/2}$ and immobile fraction data correlated with transcriptional output in the PRL-Array model. Previous reports demonstrated our ability to study transcriptional activation using RNA FISH probes that hybridize with the dsRed2 reporter gene. The EPA45 compounds (at the dose used in Table 1) were tested for their ability to induce PRL-Array reporter gene transcription. Utilizing the new version of PRL-Array cells, we can determine both agonist and inverse agonist activities of the EPA45 compounds compared to the DMSO control (significantly repressed in red box, significantly induced in green box, Figure 4A). In the original PRL-Array cell line, we showed mRNA production from the array is highly correlated with the ERα-GFP array area and found this observation also holds true with the EPA45 compounds (Figure 4B) in the PRL-Array cell model. Interestingly, raloxifene hydrochloride induced decondensation of the locus more than the other inverse agonists, but transcriptional activity was markedly suppressed; interestingly, this is in contrast with the other inverse agonists within the assay and the previously observed correlation between array area and transcriptional output.

Overall, neither $T_{1/2}$ and immobile fraction of the EPA45 compounds showed strong correlation with transcriptional output (Figures 4C and 4D, respectively); however, the data appeared to show a skewed distribution that may represent a combination of multiple distributions. We separated the compounds into those with a dsRed2 FISH intensity significantly lower than DMSO (based on p value of compound vs DMSO, red dots, Figures 4E and 4F) or significantly greater than DMSO (based on p value of compound vs DMSO, green dots, Figures 4E and 4F). When separated in this way, the inverse agonists (red dots) showed a strong negative correlation with both the $T_{1/2}$ and immobile fraction data. These data suggest that while $T_{1/2}$ and immobile fraction results are not related directly to agonism or inverse agonism, the increased $T_{1/2}$ (slower recovery) and larger immobile fraction (less recovery) can identify potent inverse agonists.

Comparison of PRL-Array and FRAPnalysis metrics and coactivator recruitment

As early coactivator recruitment is a central tenet of nuclear receptor-based transcription, we sought to determine if the recruitment of the SRC/p160 family of coactivators correlated with the PRL-Array and/or FRAP metrics. Figure 5A shows a heatmap of the SRC-1 (NCOA1), SRC-2 (NCOA2), and SRC-3 (NCOA3) loading ratios for the array inducing EPA45 compounds, ordered by mRNA induction. The loading ratio is defined as the fluorescence intensity of signal in the array mask divided by the fluorescence intensity of signal in the nucleoplasm mask. Interestingly, Raloxifene, which had the highest suppression of dsRed2 transcription, had an increased level of SRC-1 loading as compared to 4HT and the other inverse agonists. Although all three SRCs correlate at least moderately with each other, mRNA FISH intensity, and array area (Pearson's $r > 0.5$, Table S1), SRC-1 correlates most-strongly with SRC-2 (Pearson's $r = 0.858$, Figure 5B) and array area (Pearson's $r = 0.870$), and SRC-3 most-strongly correlates with mRNA FISH intensity (Pearson's $r = 0.798$, Figure 5C). None of the SRCs correlate significantly with either the $T_{1/2}$ (Figures S7A, S7C, and S7E) or immobile fraction (Figures S7B, S7D, and S7F) results. These data suggest that SRC-1, SRC-2, and SRC-3 recruitment is not a mitigating factor in determining estrogen receptor mobility; interestingly, when ER is anchored to a lacO array, the receptor-coactivator interactions are also remarkably dynamic.

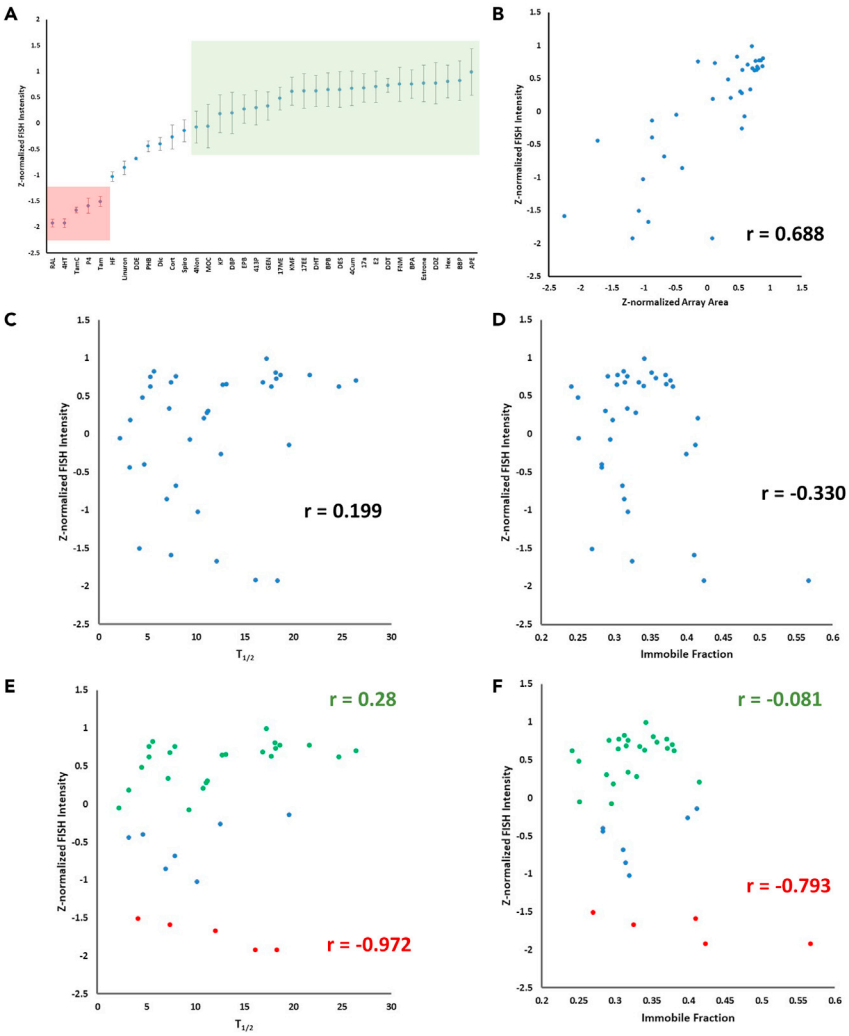

Figure 4. Correlations between FRAP and activity metrics

(A) Transcriptional activity for each array inducing EPA45 compound as measured by RNA fluorescence *in situ* hybridization of the dsRed2 reporter gene mRNA. Compounds that significantly ($p < 0.05$) repressed transcription are marked with a red box. Compounds that significantly ($p < 0.05$) induced transcription are marked in a green box. (B–F) Array-inducing EPA45 compounds in correlation plots comparing (B) array area versus FISH intensity, (C) FISH versus $T_{1/2}$, and (D) FISH intensity versus Immobile Fraction along with Pearson's (r) correlation. Correlation plots of (E) FISH intensity versus $T_{1/2}$ and (F) FISH intensity versus Immobile Fraction with compounds whose FISH induction is significantly greater than DMSO in green, significantly less than DMSO in red, and no different than DMSO itself in black. Pearson's correlation for the subgroups are labeled in their matching color. Data are represented as mean ± SD.

Differential clustering of EPA45 compounds based on PRL-Array metrics

We performed hierarchical clustering with the open source ToxPi software (Marvel et al., 2018) to group the array-inducing compounds using the seven PRL-Array metrics measured in this study (array area, mRNA FISH intensity, SRC-1 loading ratio, SRC-2 loading ratio, SRC-3 loading ratio, immobile fraction, and $T_{1/2}$) (Figure 5D). The clustering revealed five overall groups: Group 1 (blue) consists of strong agonists (i.e., E2, Estrone (Est), and Diethylstillbestrol (DES)) based on FISH intensity and array area with slower recovery time; Group 2 (orange) consists of agonists (i.e., Bisphenol A (BPA), Bisphenol B (BPB, and Kepone (KP)) faster recovery time (average $T_{1/2}$ for blue group is 17.48 ± 4.83s, average $T_{1/2}$ for orange is 7.26 ± 2.9s); Group 3 (yellow) consists of DMSO-like compounds (i.e., Dicofol (Dic) and MOC) and some antagonistic compounds (i.e., Tamoxifen (Tam) and Tamoxifen Citrate (TamC)) that induce arrays; Group 4 (purple) is the antagonist/partial group of compounds with a complete lack of SRC-2 loading (i.e., 4-hydroxytamoxifen (4HT) and progesterone (P4)); and Group 5 (green) includes only Raloxifene, which due to its high antagonistic properties, coregulator loading, and very high immobile

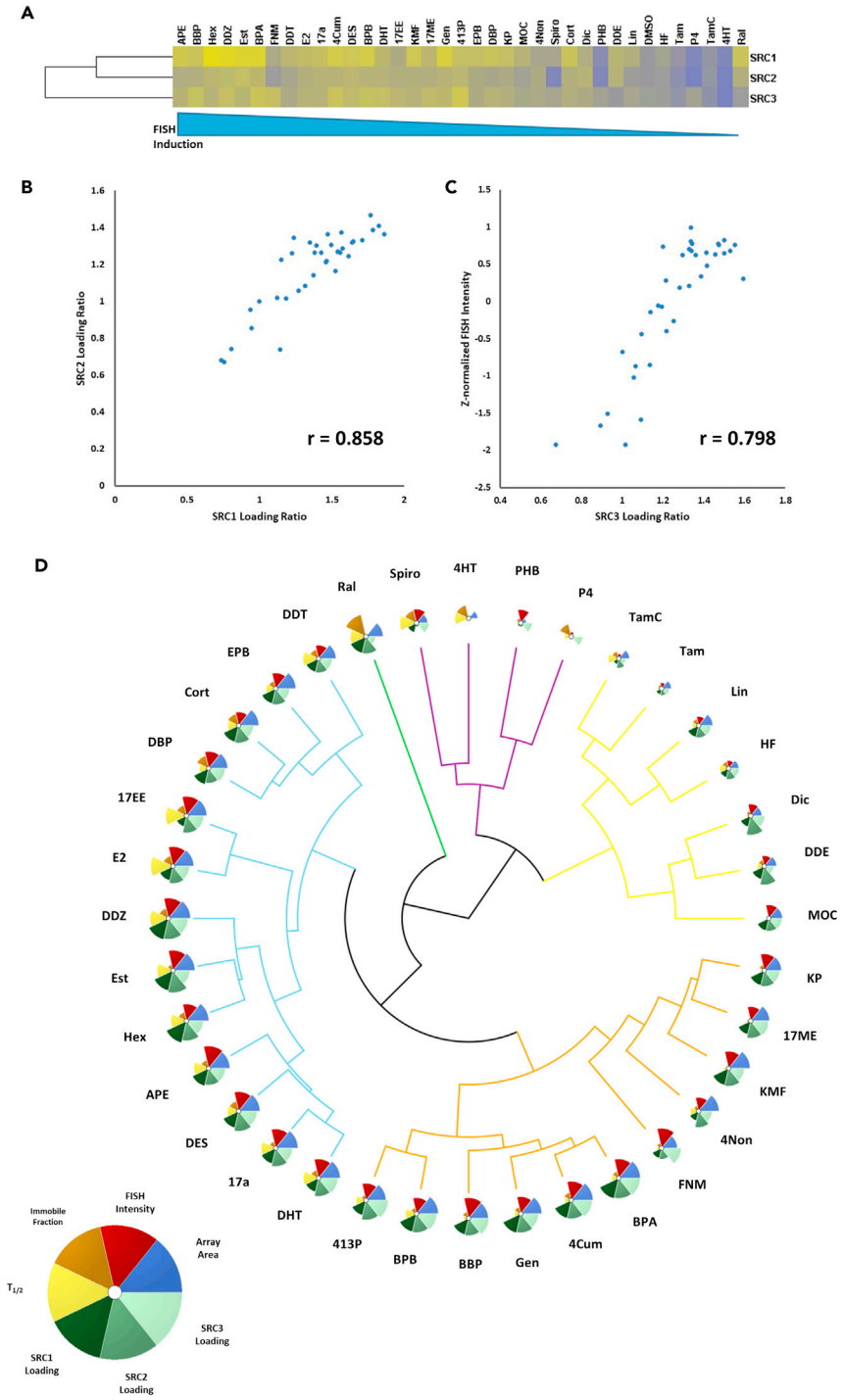

Figure 5. Coregulator recruitment to the PRL array

(A) A heatmap showing the loading ratios for SRC-1, -2, and -3 for each of the EPA45 compounds, with the compounds arranged by dsRed2 FISH induction.

(B) Correlation plot of SRC1 loading ratio versus SRC2 loading ratio.

(C) Correlation plot of SRC3 loading ratio versus FISH intensity.

(D) ToxPi hierarchical clustering of EPA45 compounds based on PRL-Array metrics: FISH Intensity, Array Area, T1/2, Immobile Fraction, SRC1 loading ratio, SRC2 loading ratio, and SRC3 loading ratio.

fraction clustered by itself. This data suggests that the group of ERα agonists can fall into two classes: (1) compounds that result in a highly mobile receptor; or, (2) compounds that result in a slower receptor, perhaps due to increased interaction with chromatin.

DISCUSSION

In this work we utilized a new variant of the previously described PRL-Array cell line: a doxycycline-inducible, C-terminal fusion of ERα that has been shown to be more sensitive than the original N-terminal fusion of ERα (i.e., ERα-GFPα:PRL-HeLa)We used the new FRAP approach to measure mobility and residency of ERα across a host of environmentally linked ligands as determined by the EPA. This is the first dataset that analyzes and compares a large cohort of environmentally relevant ligands (45 chemicals from the EPA) using FRAP and integrating the results with many other mechanistic endpoints in the ERα pathway (DNA binding, chromatin remodeling, coregulator recruitment, and gene transcription). We also developed a new image analysis pipeline to analyze multiple ROIs in FRAP experiments, called FRAPnalysis, that affords the possibility of testing a larger replicate number of cells/runs compared to typical FRAP experiments (Koulouras et al., 2018).

One interesting finding was the increased $T_{1/2}$ of ERα in the PRL-Array lines compared with other publications using similar methodology (26.4s vs 3–15s respectively (Stenoien et al., 2001a; Tanida et al., 2015; Ochiai et al., 2004; Martinez et al., 2005; Hashimoto et al., 2012)). One key difference to FRAP within the PRL-Array cell line versus a normal cell line with a GFP-tagged receptor is the presence of a greater number of ERα binding sites within a smaller nuclear volume compared to a normal nucleus, which responds ideally to reference agonists/antagonists. Another difference between the studies mentioned above are the microscopes, magnification, image times, ROI selection or type of analysis used, with any or all reasons potentially leading to different metrics. FRAP experiments with GFP-tagged androgen receptors on the MMTV array (Nenseth et al., 2014) also showed longer $T_{1/2}$s than nuclear GFP-AR (Marcelli et al., 2006) (14.9s vs 5s). Thus, the ERα-GFP:PRL-Array model affords us the ability to determine accurate residence times without using more complex methods (i.e., single molecule tracking) while still able to provide similar mobility and residence times from single molecule tracking data (Paakinaho et al., 2017).

We found a correlation between $T_{1/2}$ and immobile fraction with inverse agonist potency. While the current theories in transcription activation point to a more dynamic version of its mechanics, our data suggests that the more potent inverse agonists increase the occupancy time on DNA. This has also been observed for other nuclear receptors as slowing down the glucocorticoid receptor on the *SGK1* gene increases the potency of transcription repression (Clauss et al., 2017). Although we were focused upon ERα mobility, it is probable that changes in mobility and residency time also intersect with coactivator/corepressor interactions in transcription complexes and/or chromatin accessibility (Stenoien et al., 2001a). We see no correlation between SRC expression/recruitment and mobility, but it is possible that corepressors (i.e., NCoR/SMRT) may play a role in slowing the receptor for maximal inhibition; unfortunately, the quality tools needed to examine CoA/CoR by imaging are lacking.

We find a significant difference in mobility between compound classes (steroid vs diphenyl) binding to ERα, with the diphenyl compounds resulting in a receptor that is much more mobile. One way these compounds could be affecting mobility is through different distributions of post-translational modifications (PTMs) on ERα. Multiple kinase pathways have been shown to affect ERα DNA binding ability including AKT and PKA (Likhite et al., 2006). ERα is a phosphoprotein that can be phosphorylated on many different residues with effects on DNA Binding (Y219), and dimerization (S104/S106, S118, and S236) (Le Romancer et al., 2011), either of which could have marked effects on mobility. Changes in PTM on ERα can be induced by EDCs not only through direct binding of the EDC to ERα inducing a conformational change in the protein but also through various signaling pathways that EDCs can affect (Shanle and Xu, 2011). ERα can also be SUMOylated at multiple residues within the hinge region (K266, K268, K303, and K302) which has been shown to be vital for DNA binding (Sentis et al., 2005). EDC contribution to the SUMO pathways is not well studied but literature has shown the ability of BPA to change SUMO expression levels (Yarahalli Jayaram et al., 2020). Through changes to ERα PTMs it is possible for certain classes of EDCs to affect ERα DNA binding thus affecting mobility. When you further break down the diphenyl group into organochlorines (DDT, DDT, Methoxychlor, Fenarimol, and Dicofol) vs alkylphenols (BPA, BPB, and 4-Cumylphenol) we find no significant difference between the groups in altering ERα mobility suggesting that it may be that the two phenol rings are causing the overall shift in mobility. Although we find no significant difference between phytoestrogens (isoflavones) and pollutants (diphenyls) we do see within the groups a high level

of heterogeneous responses. In the isoflavone group, both Genistein and Kaempferol lead to a highly mobile receptor, while Apigenin and Daidzein treated led to a much slower moving receptor. We suggest that these types of comparisons, plus studies into the changes to ERα PTMs with different EDC treatments, will be important future studies to further our knowledge of EDC actions.

Finally, although our previous work with the PRL-Array has always found a very high correlation ($r \geq 0.9$) between transcription output and array area (Bolt et al., 2015), we have yet-to-find compounds that would induce chromatin decondensation and also block transcription. Within the EPA45 compounds, we found that raloxifene hydrochloride induced medium-sized arrays while suppressing mRNA production from the locus. Interestingly, raloxifene hydrochloride produced the lowest FISH intensity for the reporter gene mRNA but had the largest array area of any inverse agonist, suggesting it was able to cause a change in ERα-GFP that promoted chromatin decondensation, yet blocked RNA polymerase II recruitment or activation. This was also indicative with SRC-1 loading occurring with Raloxifene which also correlates with array area. With raloxifene belonging to a group of selective estrogen receptor modulators (compounds whose effect on ERα differ depending on the tissue type) (Patel and Bihani, 2018), our observations may be due to the HeLa background (cervical cell as opposed to breast cell) of the PRL-array. Raloxifene also causes the receptor to immobilize (observed previously in (Damdimopoulos et al., 2008)), similar to the effect of ICI (Stenoien et al., 2001b). However, unlike ICI, Raloxifene does not cause rapid receptor degradation (Schafer et al., 1999). We also discovered a ligand (Benzylbutyl Phthalate) that can induce large arrays and mRNA induction, but with FRAP metrics that are closer to the DMSO control, with rapid recovery and lower residency. These data suggest a different form of transcriptional activation and repression than those employed by standard ERα agonists/antagonists such as E2 and 4HT as visualized in the PRL-Array system. These findings showcase the utility of the PRL-Array cell line not only in clustering together large assortments of estrogenic compounds, but also the ability to discern mechanistic differences between those groups with respect to both transcriptional readout and protein dynamics.

Limitations of study

A limitation of this study is the use of an engineered cell line. The multi-copy transcription locus possesses many ER binding sites to aid in visualization and quantitation; unfortunately, the dynamics of ER binding to a native promoter is not possible by imaging, which prompted the PRL-array models that respond as expected endocrine treatments (e.g., E2, Tam, and ICI). As GFP-tagging is required for live experiments, we primarily used C-terminal tagging of ER with GFP as it was reproducibly more active than the N-terminal GFP fusion; both had similar t1/2's, with an increased immobile fraction for the C-terminal tagged receptor. Owing to the nature of the fixed vs live experiments, the same cells cannot be examined in all modalities since static FISH and antibody labeling data cannot be done live while dynamic FRAP data is only available from live imaging, so the comparisons aren't made in the same set of cells. A further limitation is with the FRAPnalysis algorithm which assumes minimal movement of the cells during the FRAP experiment window. Highly mobile cells will not work with the algorithm.

STAR★METHODS

Detailed methods are provided in the online version of this paper and include the following:

- KEY RESOURCES TABLE
- RESOURCE AVAILABILITY
  - Lead contact
  - Material availability
  - Data and code availability
- EXPERIMENTAL MODEL AND SUBJECT DETAILS
- METHOD DETAILS
  - Fluorescence *in situ* hybridization
  - Antibody labeling
  - High Throughput imaging & analysis
  - Fluorescence recovery after photo bleaching
- QUANTIFICATION AND STATISTICAL ANALYSIS
  - FRAPnalysis methodology
  - Isolation forest outlier discovery
  - Graphics and statistical analysis

SUPPLEMENTAL INFORMATION

Supplemental information can be found online at https://doi.org/10.1016/j.isci.2021.103227.

ACKNOWLEDGMENTS

M.A.M, F.S. and MGM are funded in part by NIEHS (P42ES027704). M.A.M, M.J.B., C.E.O., P.S., F.S., R.T.P. are supported via the CPRIT-funded GCC Center for Advanced Microscopy and Image Informatics (RP170719). P.S., R.T.P. and M.A.M are also supported by the CPRIT-funded Combinatorial Drug Discovery Program (RP200668). MAM is also partially funded by the GCC Center for Precision Environmental Health (P30ES030285). Imaging was supported by the CPRIT-funded GCC Center for Advanced Microscopy and Image Informatics (RP170719).

AUTHOR CONTRIBUTIONS

Conceptualization, M.J.B., P.S., F.S., and M.A.M.; Investigation, M.J.B. and C.E.O.; Methodology, M.J.B., P.S., and R.T.P.; Resources, M.G.M, P.S., and R.T.P., Writing – original draft, M.J.B.; Writing – review & editing, M.J.B., F.S. and M.A.M.; Visualization, M.J.B.; Supervision, F.S and M.A.M.; Funding Acquisition, M.A.M.

DECLARATION OF INTERESTS

The authors declare no competing interests.

Received: May 20, 2021
Revised: August 30, 2021
Accepted: September 30, 2021
Published: November 19, 2021

REFERENCES

Amita, M., Takahashi, T., Tsutsumi, S., Ohta, T., Takata, K., Henmi, N., Hara, S., Igarashi, H., Takahashi, K., and Kurachi, H. (2010). Molecular mechanism of the inhibition of estradiol-induced endometrial epithelial cell proliferation by clomiphene citrate. Endocrinology *151*, 394–405. https://doi.org/10.1210/en.2009-0721.

Bajusz, D., Racz, A., and Heberger, K. (2015). Why is Tanimoto index an appropriate choice for fingerprint-based similarity calculations? J. Cheminform *7*, 20. https://doi.org/10.1186/s13321-015-0069-3.

Bolt, M.J., Stossi, F., Callison, A.M., Mancini, M.G., Dandekar, R., and Mancini, M.A. (2015). Systems level-based RNAi screening by high content analysis identifies UBR5 as a regulator of estrogen receptor-alpha protein levels and activity. Oncogene *34*, 154–164. https://doi.org/10.1038/onc.2013.550.

Bolt, M.J., Stossi, F., Newberg, J.Y., Orjalo, A., Johansson, H.E., and Mancini, M.A. (2013). Coactivators enable glucocorticoid receptor recruitment to fine-tune estrogen receptor transcriptional responses. Nucleic Acids Res. *41*, 4036–4048. https://doi.org/10.1093/nar/gkt100.

Clauss, K., Popp, A.P., Schulze, L., Hettich, J., Reisser, M., Escoter Torres, L., Uhlenhaut, N.H., and Gebhardt, J.C.M. (2017). DNA residence time is a regulatory factor of transcription repression. Nucleic Acids Res. *45*, 11121–11130. https://doi.org/10.1093/nar/gkx728.

Damdimopoulos, A.E., Spyrou, G., and Gustafsson, J.A. (2008). Ligands differentially modify the nuclear mobility of estrogen receptors alpha and beta. Endocrinology *149*, 339–345. https://doi.org/10.1210/en.2007-0198.

De Coster, S., and van Larebeke, N. (2012). Endocrine-disrupting chemicals: associated disorders and mechanisms of action. J. Environ. Public Health *2012*, 713696. https://doi.org/10.1155/2012/713696.

de Hoon, M.J.L., Imoto, S., Nolan, J., and Miyano, S. (2004). Open source clustering software. Bioinformatics *20*, 1453–1454.

Demsar, J., Curk, T., Erjavec, A., Gorup, C., Hocevar, T., Multinovic, M., Mozina, M., Polajnar, M., Toplk, M., Staric, A., Stajdohar, M., et al. (2013). Orange: data mining in Python. J. Mach. Learn. Res. *14*, 2349–2353.

Govindaraj, K., Hendriks, J., Lidke, D.S., Karperien, M., and Post, J.N. (2019). Changes in fluorescence recovery after photobleaching (FRAP) as an indicator of SOX9 transcription factor activity. Biochim. Biophys. Acta Gene Regul. Mech. *1862*, 107–117. https://doi.org/10.1016/j.bbagrm.2018.11.001.

Guan, J., Zhou, W., Hafner, M., Blake, R.A., Chalouni, C., Chen, I.P., De Bruyn, T., Giltnane, J.M., Hartman, S.J., Heidersbach, A., and Houtman, R. (2019). Therapeutic ligands antagonize estrogen receptor function by impairing its mobility. Cell *178*, 949–963.e918. https://doi.org/10.1016/j.cell.2019.06.026.

Hashimoto, T., Matsuda, K., and Kawata, M. (2012). Scaffold attachment factor B (SAFB)1 and SAFB2 cooperatively inhibit the intranuclear mobility and function of ERalpha. J. Cell Biochem. *113*, 3039–3050. https://doi.org/10.1002/jcb.24182.

Horner-Glister, E., Maleki-Dizaji, M., Guerin, C.J., Johnson, S.M., Styles, J., and White, I.N. (2005). Influence of oestradiol and tamoxifen on oestrogen receptors-alpha and -beta protein degradation and non-genomic signalling pathways in uterine and breast carcinoma cells. J. Mol. Endocrinol. *35*, 421–432. https://doi.org/10.1677/jme.1.01784.

Judson, R.S., Magpantay, F.M., Chickarmane, V., Haskell, C., Tania, N., Taylor, J., Xia, M., Huang, R., Rotroff, D.M., Filer, D.L., and Houck, K.A. (2015). Integrated model of chemical perturbations of a biological pathway using 18 in vitro high-throughput screening assays for the estrogen receptor. Toxicol. Sci. *148*, 137–154. https://doi.org/10.1093/toxsci/kfv168.

Kornhuber, M., Dunst, S., Schonfelder, G., and Oelgeschlager, M. (2021). The E-Morph Assay: identification and characterization of environmental chemicals with estrogenic activity based on quantitative changes in cell-cell contact organization of breast cancer cells. Environ. Int. *149*, 106411. https://doi.org/10.1016/j.envint.2021.106411.

Koulouras, G., Panagopoulos, A., Rapsomaniki, M.A., Giakoumakis, N.N., Taraviras, S., and Lygerou, Z. (2018). EasyFRAP-web: a web-based tool for the analysis of fluorescence recovery after photobleaching data. Nucleic Acids Res. *46*, W467–W472. https://doi.org/10.1093/nar/gky508.

Le Romancer, M., Poulard, C., Cohen, P., Sentis, S., Renoir, J.M., and Corbo, L. (2011). Cracking

the estrogen receptor's posttranslational code in breast tumors. Endocr. Rev. *32*, 597–622. https://doi.org/10.1210/er.2010-0016.

Likhite, V.S., Stossi, F., Kim, K., Katzenellenbogen, B.S., and Katzenellenbogen, J.A. (2006). Kinase-specific phosphorylation of the estrogen receptor changes receptor interactions with ligand, deoxyribonucleic acid, and coregulators associated with alterations in estrogen and tamoxifen activity. Mol. Endocrinol. *20*, 3120–3132. https://doi.org/10.1210/me.2006-0068.

Liu, F.T., Zhou Z.H.. (2008). Isolation forest. 2008 Eighth IEEE International Conference on Data Mining, 413-422.

Marcelli, M., Stenoien, D.L., Szafran, A.T., Simeoni, S., Agoulnik, I.U., Weigel, N.L., Moran, T., Mikic, I., Price, J.H., and Mancini, M.A. (2006). Quantifying effects of ligands on androgen receptor nuclear translocation, intranuclear dynamics, and solubility. J. Cell Biochem. *98*, 770–788. https://doi.org/10.1002/jcb.20593.

Martinez, E.D., Rayasam, G.V., Dull, A.B., Walker, D.A., and Hager, G.L. (2005). An estrogen receptor chimera senses ligands by nuclear translocation. J. Steroid Biochem. Mol. Biol. *97*, 307–321. https://doi.org/10.1016/j.jsbmb.2005.06.033.

Marvel, S.W., To, K., Grimm, F.A., Wright, F.A., Rusyn, I., and Reif, D.M. (2018). ToxPi graphical user interface 2.0: dynamic exploration, visualization, and sharing of integrated data models. BMC Bioinform. *19*, 80. https://doi.org/10.1186/s12859-018-2089-2.

Nenseth, H.Z., Dezitter, X., Tesikova, M., Mueller, F., Klokk, T.I., Hager, G.L., and Saatcioglu, F. (2014). Distinctly different dynamics and kinetics of two steroid receptors at the same response elements in living cells. PLoS One *9*, e105204. https://doi.org/10.1371/journal.pone.0105204.

Ochiai, I., Matsuda, K., Nishi, M., Ozawa, H., and Kawata, M. (2004). Imaging analysis of subcellular correlation of androgen receptor and estrogen receptor alpha in single living cells using green fluorescent protein color variants. Mol. Endocrinol. *18*, 26–42. https://doi.org/10.1210/me.2002-0262.

Ozturk, H., Ozkirimli, E., and Ozgur, A. (2016). A comparative study of SMILES-based compound similarity functions for drug-target interaction prediction. BMC Bioinform. *17*, 128. https://doi.org/10.1186/s12859-016-0977-x.

Paakinaho, V., Presman, D.M., Ball, D.A., Johnson, T.A., Schiltz, R.L., Levitt, P., Mazza, D., Morisaki, T., Karpova, T.S., and Hager, G.L. (2017). Single-molecule analysis of steroid receptor and cofactor action in living cells. Nat. Commun. *8*, 15896. https://doi.org/10.1038/ncomms15896.

Patel, H.K., and Bihani, T. (2018). Selective estrogen receptor modulators (SERMs) and selective estrogen receptor degraders (SERDs) in cancer treatment. Pharmacol. Ther. *186*, 1–24. https://doi.org/10.1016/j.pharmthera.2017.12.012.

Powles, T.J. (2006). Prevention of breast cancer using selective oestrogen receptor modulators (SERMs). Breast Cancer Res. *8*, 111. https://doi.org/10.1186/bcr1601.

Reif, D.M., Martin, M.T., Tan, S.W., Houck, K.A., Judson, R.S., Richard, A.M., Knudsen, T.B., Dix, D.J., and Kavlock, R.J. (2010). Endocrine profiling and prioritization of environmental chemicals using ToxCast data. Environ. Health Perspect. *118*, 1714–1720. https://doi.org/10.1289/ehp.1002180.

Rochester, J.R. (2013). Bisphenol A and human health: a review of the literature. Reprod. Toxicol. *42*, 132–155. https://doi.org/10.1016/j.reprotox.2013.08.008.

Rudnik, V., Sanyal, A., Syed, F.A., Monroe, D.G., Spelsberg, T.C., Oursler, M.J., and Khosla, S. (2008). Loss of ERE binding activity by estrogen receptor-alpha alters basal and estrogen-stimulated bone-related gene expression by osteoblastic cells. J. Cell Biochem *103*, 896–907. https://doi.org/10.1002/jcb.21459.

Saldanha, A.J. (2004). Java Treeview—extensible visualization of microarray data. Bioinformatics *20*, 3246–3248.

Schafer, J.I., Liu, H., Tonetti, D.A., and Jordan, V.C. (1999). The interaction of raloxifene and the active metabolite of the antiestrogen EM-800 (SC 5705) with the human estrogen receptor. Cancer Res. *59*, 4308–4313. https://www.ncbi.nlm.nih.gov/pubmed/10485477.

Sentis, S., Le Romancer, M., Bianchin, C., Rostan, M.C., and Corbo, L. (2005). Sumoylation of the estrogen receptor alpha hinge region regulates its transcriptional activity. Mol. Endocrinol. *19* (11), 2671–2684. https://doi.org/10.1210/me.2005-0042.

Shanle, E.K., and Xu, W. (2011). Endocrine disrupting chemicals targeting estrogen receptor signaling: identification and mechanisms of action. Chem. Res. Toxicol. *24*, 6–19. https://doi.org/10.1021/tx100231n.

Sharp, Z.D., Mancini, M.G., Hinojos, C.A., Dai, F., Berno, V., Szafran, A.T., Smith, K.P., Lele, T.T., Ingber, D.E., and Mancini, M.A.((2006). Estrogen-receptor-alpha exchange and chromatin dynamics are ligand- and domain-dependent. J. Cell Sci *119*, 4101–4116. https://doi.org/10.1242/jcs.03161.

Simpson, E.R., Mahendroo, M.S., Means, G.D., Kilgore, M.W., Hinshelwood, M.M., Graham-Lorence, S., Amarneh, B., Ito, Y., Fisher, C.R., Michael, M.D., and Mendelson, C.R. (1994). Aromatase cytochrome P450, the enzyme responsible for estrogen biosynthesis. Endocr. Rev. *15*, 342–355. https://doi.org/10.1210/edrv-15-3-342.

Stavreva, D.A., Varticovski, L., Levkova, L., George, A.A., Davis, L., Pegoraro, G., Blazer, V., Iwanowicz, L., and Hager, G.L. (2016). Novel cell-based assay for detection of thyroid receptor beta-interacting environmental contaminants. Toxicology *368–369*, 69–79. https://doi.org/10.1016/j.tox.2016.08.012.

Stenoien, D.L., Nye, A.C., Mancini, M.G., Patel, K., Dutertre, M., O'Malley, B.W., Smith, C.L., Belmont, A.S., and Mancini, M.A.((2001a). Ligand-mediated assembly and real-time cellular dynamics of estrogen receptor alpha-coactivator complexes in living cells. Mol. Cell Biol. *21*, 4404–4412. https://doi.org/10.1128/MCB.21.13.4404-4412.2001.

Stenoien, D.L., Patel, K., Mancini, M.G., Dutertre, M., Smith, C.L., O'Malley, B.W., and Mancini, M.A. (2001b). FRAP reveals that mobility of oestrogen receptor-alpha is ligand- and proteasome-dependent. Nat. Cell Biol. *3*, 15–23. https://doi.org/10.1038/35050515.

Stossi, F., Bolt, M.J., Ashcroft, F.J., Lamerdin, J.E., Melnick, J.S., Powell, R.T., Dandekar, R.D., Mancini, M.G., Walker, C.L., Westwick, J.K., and Mancini, M.A.((2014). Defining estrogenic mechanisms of bisphenol A analogs through high throughput microscopy-based contextual assays. Chem. Biol. *21*, 743–753. https://doi.org/10.1016/j.chembiol.2014.03.013.

Tanida, T., Matsuda, K.I., Yamada, S., Hashimoto, T., and Kawata, M. (2015). Estrogen-related receptor beta reduces the subnuclear mobility of estrogen receptor alpha and suppresses estrogen-dependent cellular function. J. Biol. Chem. *290*, 12332–12345. https://doi.org/10.1074/jbc.M114.619098.

van Royen, M.E., Farla, P., Mattern, K.A., Geverts, B., Trapman, J., and Houtsmuller, A.B. (2009). Fluorescence recovery after photobleaching (FRAP) to study nuclear protein dynamics in living cells. Methods Mol. Biol. *464*, 363–385. https://doi.org/10.1007/978-1-60327-461-6_20.

Vasquez, Y.M. (2018). Estrogen-regulated transcription: mammary gland and uterus. Steroids *133*, 82–86. https://doi.org/10.1016/j.steroids.2017.12.014.

Xu, T., Kirkpatrick, A., Toperzer, J., Ripp, S., and Close, D. (2019). Improving estrogenic compound screening efficiency by using self-modulating, continuously bioluminescent human cell bioreporters expressing a synthetic luciferase. Toxicol. Sci. *168*, 551–560. https://doi.org/10.1093/toxsci/kfz004.

Yarahalli Jayaram, V., Baggavalli, S., Reddy, D., Sistla, S., and Malempati, R. (2020). Effect of endosulfan and bisphenol A on the expression of SUMO and UBC9. Drug Chem. Toxicol. *43*, 637–644. https://doi.org/10.1080/01480545.2018.1526179.

Zoeller, R.T., Brown, T.R., Doan, L.L., Gore, A.C., Skakkebaek, N.E., Soto, A.M., Woodruff, T.J., and Vom Saal, F.S. (2012). Endocrine-disrupting chemicals and public health protection: a statement of principles from the Endocrine Society. Endocrinology *153*, 4097–4110. https://doi.org/10.1210/en.2012-1422.

STAR★METHODS

KEY RESOURCES TABLE

REAGENT or RESOURCE	SOURCE	IDENTIFIER
Antibodies		
SRC-1 Antibody	BD Labs	612378; RRID AB_399738
SRC-2 Antibody	BD Labs	610895; RRID: AB_398298
SRC-3 Antibody	Mancini Lab	528-F12
Goat Anti Mouse Alexa Fluor 647	ThermoFisher	A48289
Chemicals, peptides, and recombinant proteins		
EPA45 Compound Set	Dr. Keith Houck (EPA)	
Experimental models: Cell lines		
ERα-GFP:PRL-HeLa	Mancini Lab	
Software and algorithms		
Pipeline Pilot Image Analysis software	Biovia	https://www.3ds.com/products-services/biovia/products/data-science/pipeline-pilot/
FRAPnalysis algorithm	Pankaj Singh	https://github.com/pankajmath/FRAPanalysis
ToxPi software	Reif et al. (2010)	Toxpi.org
Cluster 3.0	de Hoon et al. (2004)	http://bonsai.hgc.jp/~mdehoon/software/cluster/software.htm
Java Tree Viewer	Aj. 2005	http://jtreeview.sourceforge.net/
Orange software	Demsar et al. (2003)	https://orangedatamining.com/
Other		
dsRED2 FISH Probe	LGC Biosearch	Custom

RESOURCE AVAILABILITY

Lead contact

Further information and requests for resources and reagents should be directed to and will be fulfilled by the lead contact, Michael Mancini (mancini@bcm.edu).

Material availability

This study did not generate new unique reagents.

Data and code availability

All data reported in this paper will be shared by the lead contact upon request.

All original code has been deposited at Github and is publicly available as of the date of publication. DOIs are listed in the Key resources table.

Any additional information required to reanalyze the data reported in this paper is available from the lead contact upon request.

EXPERIMENTAL MODEL AND SUBJECT DETAILS

All experiments were performed with ERα-GFP:PRL-HeLa (PRL-Array) cells which are similar to those used in Bolt et al. (2015), but the GFP is now on the C-terminus, and expression is tightly controlled by doxycycline Cells were maintained in phenol red-free Dulbecco's modified Eagle's medium containing 10% fetal bovine serum (FBS), 200 μg/ml Hygromycin, and 100 μg/ml G418. Cells were plated for 48 h in 5% charcoal-stripped FBS, phenol red free Dulbecco's modified Eagle's medium before treatment on Greiner 384-well

optical bottom plates, or 8-well chamber slides. To initiate ERα-GFP expression, cells were treated with doxycycline (1 μg/ml) 24 hours before experimental treatment.

METHOD DETAILS

Fluorescence *in situ* hybridization

Cells in a 384-well plate were fixed in EM-grade 4% paraformaldehyde in RNAse-free phosphate-buffered saline for 20 min and then permeabilized with 70% ethanol in RNAse-free water at 4°C overnight. Cells were washed in wash buffer (WB, 2X SSC and 10% formamide) followed by hybridization in hybridization buffer (0.1 g dextran sulfate, 1ml of 20X SSC buffer, 1ml of formamide and 8ml of nuclease-free water) with a dsRED2 RNA probe (LGC Biosearch Technologies, diluted 1:500) overnight at 37°C. Following probe hybridization, cells were washed with WB for 30 minutes, followed by 2X SSC buffer containing DAPI for 30 min. Cells were left in 2X SSC for imaging.

Antibody labeling

Cells were fixed in 4% formaldehyde (EM-grade) in phosphate-buffered saline containing magnesium and calcium for 20 min at room temperature, quenched with 100 nM ammonium chloride for 10 min, and then permeabilized with 0.5% Triton X-100 for 15 min. Cells were incubated in 5% milk in PBS for 1 hour, followed by overnight incubation with primary antibody (SRC-1 [BD labs 612378] 0.5 μg/ml, SRC-2 [BD labs 610895] 0.5 μg/ml, SRC-3 [in house generated 528-F12] 1:500) diluted in blocking buffer. Cells were washed with blocking buffer and then incubated with secondary antibody (Anti-Mouse 647, 1 μg/ml, ThermoFischer) for 1 hour in diluted in TBST, followed by another formaldehyde fix and quench step as mentioned above to stabilize antigen localizations. Lastly, cells were incubated with DAPI (1 μg/ml) for 5 minutes. Cells were left in PBS for imaging.

High Throughput imaging & analysis

PRL-Array cells were imaged on an ImageXpress Micro (Molecular Devices) high throughput confocal microscope with an 20X/0.75 NA with 7 z-stacks at 1mm intervals in the GFP and FISH channels, or GFP and SRC antibody labeling without image binning. Image analysis was performed using a custom workflow developed with the imaging collection within the Pipeline Pilot enterprise scale GUI-based programming platform (PLP, *BIOVIA*) as described previously (Bolt et al., 2013). In brief, images and metadata data are first read into PLP and then background corrected. Next, the ERα-GFP and FISH z-stacked images are projected using the "stack focuser" plug-in integrated into PLP. The DAPI signal is then used to define nuclear regions that are subsequently expanded by 8 μm to include analysis of the perinuclear spaces. Array segmentation is done using a local subtraction (per nuclear area) peak-finding algorithm followed by user-defined filtering to minimize false-positives. Count, morphometric and intensity-based features are subsequently measured for each channel and mask combination. The Loading Ratio, for any antibody labeling, is equal to the average fluorescence intensity at the array divided by the average fluorescence intensity in the nucleoplasm.

Fluorescence recovery after photo bleaching

FRAP experiments were performed on a Leica SP-8 confocal microscope combined with a Tokai Hit STX series stage top incubator system. During imaging cells were kept at 37°C with 5% CO_2. Imaging was performed with a white light laser set to 484 nm (2% power) using a 63X/1.40 NA oil objective on a 2X zoom. Three pre-bleach images were taken. ROIs were then bleached with the 405 nm laser (50% power) with a one second burst. The cells were then imaged every 2.21 seconds for 2 minutes. ROIs were selected over the transcriptional array in cells that were not touching the edge of the field. For each compound, a total of 30 cells were photobleached (3 random fields containing 5 cells each, done in two biological replicates).

QUANTIFICATION AND STATISTICAL ANALYSIS

FRAPnalysis methodology

To automatically find the FRAP'ed regions, we took advantage of the fact that the last pre-bleached (PreB) image and the first post-bleached (PB) image would be the same except for the bleached regions (FRAP regions). First, we used Gaussian filtering to blur the images and subtracted the blurred PB image from the blurred PreB image. To obtain the FRAP regions, we segmented the subtracted image using Otsu method (Otsu N, 1979), filled the holes, and removed small debris. For each estimated FRAP region, we

found the pixel with the maximum value in the subtracted image and used that pixel as the center to draw a circle of fixed radius. These circular regions become our FRAP regions of interest (ROI) in the image. Once we identified these FRAP regions, we calculated the mean intensity value in the ROIs for each time point and normalized it to the mean intensity in the first pre-bleached image. Next, we corrected for photobleaching. We segmented all the cells in the last pre-bleached image and for each cell that does not contain any FRAP regions, we selected the intersection of the segmented cell and a square region with centroid of the cell being its center, defining the ROI. We computed the mean intensity value at all the time points for all regions of interest. Next, we normalized these mean intensities to the initial mean intensity for each and obtained the median of these normalized intensities for each time point, followed by modeling the photobleaching rate if the bleach follows a single negative exponential decay given by:

$I(t) = I(0)\, e^{-\alpha t}$, where $I(t)$ is the median of the normalized intensities at time t, $I(0) = 1$, and α is the rate of photobleaching. Thus, the image intensities can be corrected by $corrected\_image\_intensity(t) = image\_intensity(t)e^{at}$.

For each FRAP region, we corrected the normalized mean intensities for photobleaching that may have occurred during acquisition not due to the bleaching laser but caused by the imaging laser. Assuming the FRAP recovery curve follows $R(t) = b\, e^{-dt} + c$, we obtained the optimal values of b, c, and d for each region. The mobile fraction is given by $a = R(T)$, where T is the last time point. Thus, the immobile fraction is $1 - R(T)$ and half-time to recovery is calculated by $\tau_{1/2} = -\frac{1}{d} ln\left(\frac{a-c}{b}\right) + s$, where s is the time taken to bleach the FRAP region.

Isolation forest outlier discovery

Outlier discovery using the isolation forest model was used as previously described (Liu and Zhou, 2008). Isolation forest is an unsupervised learning algorithm that takes advantage of the fact that outliers belong to a small group of data points, and they have very different feature values compared to those of normal instances. It explicitly isolates anomalies instead of profiling and constructing normal points and regions by assigning a score to each data point.

Graphics and statistical analysis

All graphics were made using Microsoft Excel unless otherwise stated. The heat map in Figure 1 was made in data analysis software Orange (Demsar et al., 2013). The heat map in Figure 5 was made using open source software Cluster 3.0 with Java Tree Viewer (Saldanha, 2004; de Hoon et al., 2004). Figure 5C was created using the ToxPi software (toxpi.org (Marvel et al., 2018; Reif et al., 2010)). p value was determined using student's t-test for single comparisons or one-way ANOVA for independent samples and a Tukey HSD post-hoc test for comparisons across multiple samples.